Myosin-Driven Intercellular Transportation of Wheat Germ Agglutinin Mediated by Membrane Nanotubes between Human Lung Cancer Cells

Zhi-Gang Wang, Shu-Lin Liu, Zhi-Quan Tian, Zhi-Ling Zhang, Hong-Wu Tang, and Dai-Wen Pang*

Key Laboratory of Analytical Chemistry for Biology and Medicine (Ministry of Education), College of Chemistry and Molecular Sciences, State Key Laboratory of Virology, and Wuhan Institute of Biotechnology, Wuhan University, Wuhan 430072, P.R. China

ABSTRACT Membrane nanotubes can facilitate direct intercellular communication between cells and provide a unique channel for intercellular transfer of cellular contents. However, the transport mechanisms of membrane nanotubes remain poorly understood between cancer cells. Also largely unknown is the transport pattern mediated by membrane nanotubes. In this work, wheat germ agglutinin (WGA), a widely used drug carrier and potential antineoplastic drug, was labeled with quantum dots (QDs-WGA) as a model for exploring the intercellular transportation *via* membrane nanotubes. We found that membrane nanotubes allowed effective transfer of QDs-WGA. Long-term single-particle tracking indicated that the movements of QDs-WGA exhibited a slow and directed motion pattern in nanotubes. Significantly, the transport of QDs-WGA was driven by myosin molecular motors in an active and unidirectional manner. These results contribute to a better understanding of cell-to-cell communication for cancer research.

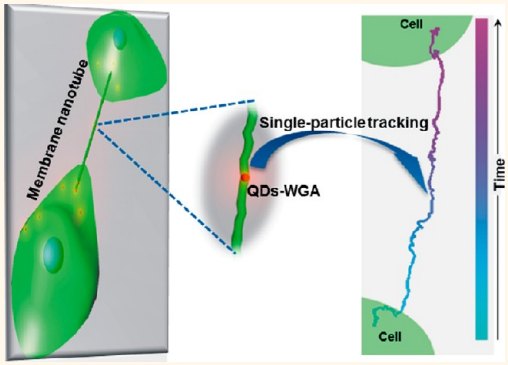

KEYWORDS: membrane nanotubes cancer cells wheat germ agglutinin quantum dots intercellular transportation myosin motors

Intercellular communication can regulate the balance between proliferation and apoptosis of cells, which plays a crucial role in cancer cell coordination and tumor invasion. To date, most researches have focused on the gap junctional intercellular communication between cancer cells.[1,2] Membrane nanotubes, as recently discovered membranous tethers between cells, attract keen interest due to their ability to facilitate direct intercellular communication, signaling and the spread of pathogens.[3−8] These tubular structures have been found between various cell types, including neuronal cells, immune cells, and cancer cells as well as other types of cells, both *in vivo* and *in vitro*.[3,9−12] More recently, some researchers have reported that the cellular contents, such as endosomes, mitochondria, and Golgi vesicles, could transfer between cancer cells through membrane nanotubes.[12,13] However, many questions regarding the transport pattern of biomolecules *via* nanotubes remain poorly understood, and little is known about the transport mechanism involved in the nanotubes between cancer cells.

Herein, we chose wheat germ agglutinin (WGA) as a model for exploring the intercellular transportation *via* membrane nanotubes between human lung cancer A549 cells. WGA can specifically recognize *N*-acetylglucosamine and sialic acid moieties, and has been widely used as a drug carriers and potential antineoplastic drugs in biology and medicine.[14−16] Researching on intercellular transportation of WGA not only helps to reveal the transport mechanism in membrane nanotubes, but also provides insights into drug delivery between cancer cells.

In this work, we labeled WGA with quantum dots (QDs) for live-cell imaging. Combining with the high brightness and excellent

* Address correspondence to dwpang@whu.edu.cn.

Received for review August 16, 2012 and accepted October 26, 2012.

Published online October 26, 2012
10.1021/nn303729r

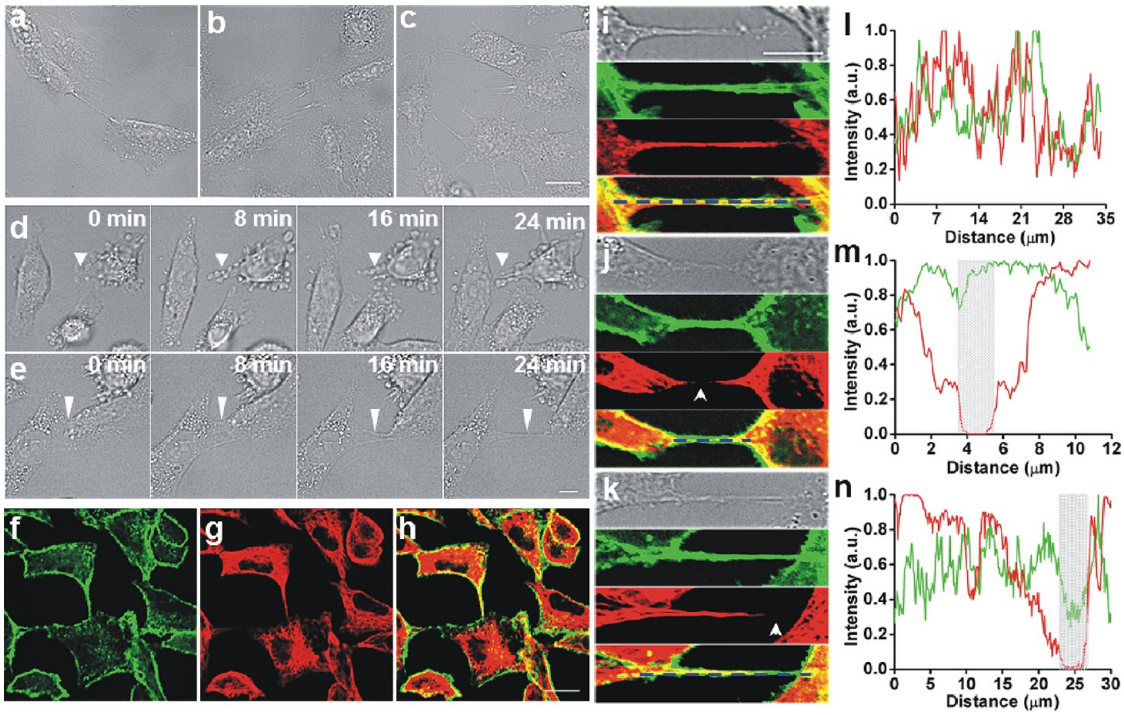

Figure 1. Membrane nanotubes can form between human lung carcinoma A549 cells (a–c) Three types of nanotubes exist among A549 cells. (a) Single membrane nanotube readily forms between two cells (n = 134). (b) Multiple membrane nanotubes connect surrounding cells (n = 62). (c) Membrane nanotubes branch out and connect several cells to form a network (n = 33). (d, e) Two distinct routes can result in membrane nanotubes formation. (d) A dynamic protrusion from one cell (the white arrows) was stretching out, connecting to a neighboring cell and forming a new nanotube. (e) The conjoint cells were moving apart, and drawing out a membrane nanotube (the white arrows). Fixed A549 cells were immunolabeled with phalloidin–fluorescein isothiocyanate (FITC) (f), an antibody against α-tubulin (g). (h) The overlapped image of panels f and g indicates that the nanotubes contain both F-actin and microtubules. (i–n) Membrane nanotubes are composed of F-actin (green) and microtubule (red) in three ways. F-actin is ubiquitous throughout the whole of the nanotubes (i–k), but a microtubule can exist in the whole (i, n = 30), both ends (j, n = 6), or one end (k, n = 5) of the nanotubes. (l–n) The cross-line scans of the fluorescence intensities of the merge images (the blue lines, i–k) show the distribution of the F-actin and microtubule signals, respectively. The white arrows (j, k) and shadow areas (m, n) indicate the absent sites of microtubules. The scale bars represent 20 μm in panels a–e, and 10 μm in panels f–k.

photostability of QDs,[17–19] we monitored the entire transport process of quantum dots-labeled wheat germ agglutinin (QDs-WGA) in nanotubes and dissected the transport behaviors of the QDs-WGA in detail by real-time single-particle tracking (SPT). We found that membrane nanotubes allowed effective transfer of the QDs-WGA between cancer cells. The transportation of the QDs-WGA in the membrane nanotubes was driven by myosin molecular motors in an active and unidirectional manner. These results lead us to propose that membrane nanotubes provide an underappreciated route for intercellular transportation between cancer cells, which may contribute to a better understanding of cell-to-cell communication for cancer research.

RESULTS AND DISCUSSION

Formation and Components of Membrane Nanotubes. To study the cell-to-cell communication *via* membrane nanotubes between living cancer cells, we chose the human lung carcinoma A549 cells as a model. We observed that membrane nanotubes existed between A549 cells and exhibited several differences in morphology. Cells were generally connected by a single nanotube (n = 134) (Figure 1a), multiple nanotubes (n = 62) (Figure 1b), or branched nanotubes (n = 8) (Figure 1c). The filamentous networks (n = 33) consisting of cells intricately interconnected by nanotubes also could be observed (Figure 1c). After 12 h incubation, approximately 11% of A549 cells (n = 2038) could be connected *via* membrane nanotubes (n = 216) which had a diameter ranging from 0.4 to 1.5 μm and a length ranging from 10 to 105 μm roughly (see Supporting Information, Figure S1). Using time-lapse microscopy, two dramatic distinct forming processes of membrane nanotubes were visualized. First, in a 24-min period, a dynamic filopodia-like protrusion from one cell was stretched out, extending unceasingly until connecting to a neighboring cell (Figure 1d). Second, in the same period, the conjoint cells were moving apart, and drawing out a membrane nanotube from the diverging cells (Figure 1e). Such processes were mutually compatible and could occur simultaneously, consistent with previous reports.[3] Occasionally, we noticed that the stretching or drawing of membrane nanotubes lasted for some time until rupture (n = 5), indicating that the formation of

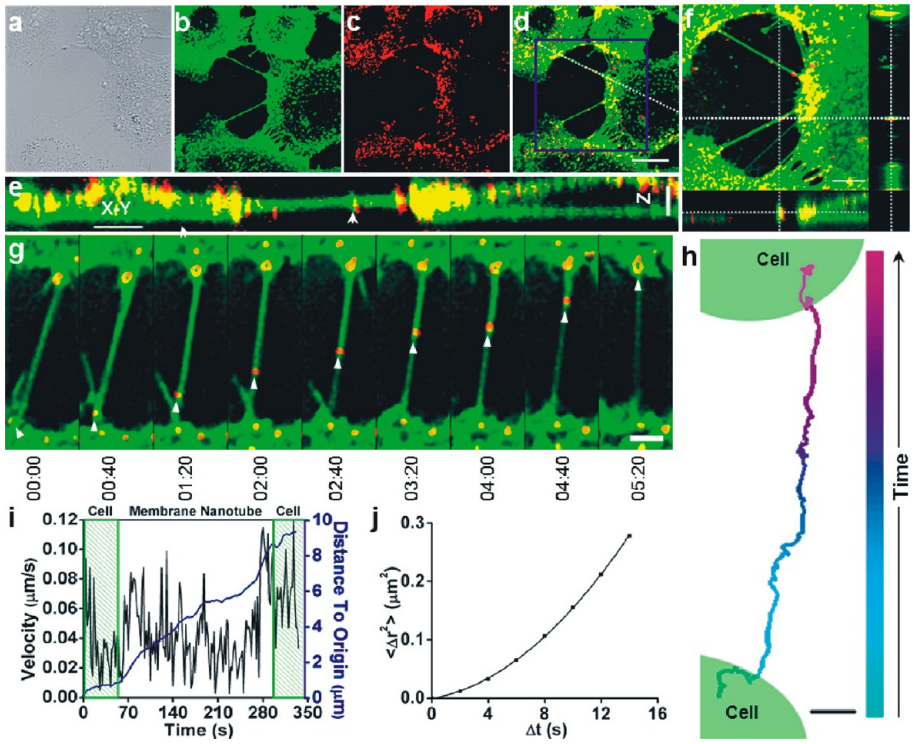

Figure 2. Quantum dots-labeled wheat germ agglutinin (QDs-WGA) moves from cell-to-cell along the membrane nanotube. The bright-field image of the membrane nanotube between A549 cells is shown in panel a. The cells stained with DiO membrane dye were incubated with QDs-WGA at 37 °C for 30 min. Fluorescence images of DiO membrane dye (b), QDs-WGA (c), and the merge image (d) are displayed. The profile image (e) of the nanotube (the white line in d) and orthogonal slice view (f) (the blue rectangular region of panel d) indicate the QDs-WGA was in the nanotube between two cells. (g) Snapshots demonstrate the QDs-WGA (the white arrows) moving from one cell to another cell along the nanotube. The time format is minutes:seconds. (see Supporting Information Movie S2). (h) Shown is the whole trajectory of the particle in panel g. (i) Velocity and distance to origin *vs* time plots are displayed. The green shadows imply the time scales in the cell bodies. (j) Mean square displacement ($\langle \Delta r^2 \rangle$) *vs* time ($\Delta t$) plot was calculated by using the points of the trajectory in the nanotube. The line is the fit to $\langle \Delta r^2 \rangle = 4D\Delta t + (V\Delta t)^2 +$ constant with $D = 0.001\ \mu m^2/s$ and $V = 0.033\ \mu m/s$ (D and V are the diffusion coefficient and fitting velocity, and the constant term is due to noise). The scale bars represent 20 μm in a–d, 10 μm in f and e, 2 μm in g, and 1 μm in h.

membrane nanotubes was a dynamic and ever-changing process.

The components of nanotubes were diverse depending on the cell types.[20,21] To detect the components of membrane nanotubes between A549 cells, F-actin and α-tubulin were immunolabeled with FITC-conjugated phalloidin and an antibody against α-tubulin, respectively (Figure 1f–h). F-actin was almost ubiquitous throughout the whole of the nanotubes (n = 41). However, a microtubule could exist in the whole (73%) (Figure 1i), both ends (15%) (Figure 1j), and one end (12%) (Figure 1k) of the nanotubes. The cross-line scans of the merge images (Figure 1l–n) explicitly suggested that membrane nanotubes were composed of F-actin and microtubules in three different forms, which raised the question of how the differences were generated. Actin filaments, one of the main components of the cytoskeleton, are tightly apposed to the plasma membrane,[22] which always are detected in nanotubes of various cell types.[3,6,12,23,24] However, microtubules exist only in the nanotubes of cardiac myoblast and human prostate cancer cells.[12,24] The different distributions of microtubules may be caused by the conjoint or fracture site during the forming and rupturing process. When the connection has just completed, the microtubule may not join thoroughly to another cell, which will result in the existence of a microtubule in one end or two ends of the nanotubes. Besides, when cells connected by a nanotube move apart, the overstretched nanotube will also cause the structural imperfection of the microtubule.

Imaging QDs-WGA in Membrane Nanotubes. One extraordinary feature of membrane nanotubes is to traffic organelles or nanoparticles between cells. Herein, to investigate the transport ability of membrane nanotubes between A549 cells, we used QDs-WGA as a paradigm, which also could reveal the mechanism for drug delivery between cancer cells.[25] QDs-WGA was dispersed evenly in the membrane dye DiO-stained A549 cells after 30 min incubation at 37 °C (Figure 2a–c). By contrast, we treated the cells with streptavidin-conjugated QDs (SA-QDs, see Supporting Information, Figure S2) alone in the negative control experiment. A very weak fluorescence signal was observed in the cells (see Supporting Information, Figure S3), suggesting that QDs-WGA probes bound to the receptor of WGA on the cell surface specifically. Our experiments also confirmed that SA-QDs were barely

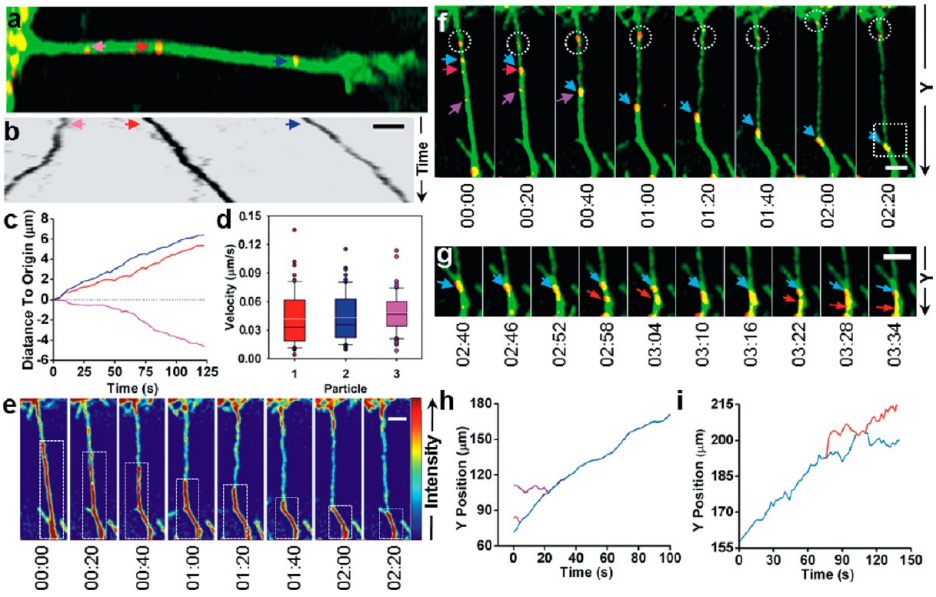

Figure 3. Multiple QDs-WGAs were transported in membrane nanotubes in special ways. Snapshot of QDs-WGAs moving in the nanotube (the arrows, a) and the corresponding kymograph image (b) show that QDs-WGAs can move along the same nanotube simultaneously in different directions. The red and blue arrows indicate that the QDs-WGAs move in the same direction and the pink arrow is in the reverse direction (see Supporting Information Movie S3) (n = 15). (c) Shown is the distance to origin (the starting positions at first frame) of the QDs-WGAs. (d) Box plots illustrate the distribution of instantaneous velocity of QDs-WGAs (P = 0.76, one-way ANOVA). The arrow colors shown in panels a and b are consistent with the plot colors in panels c and d. (e) Snapshots indicate the DiO-stained membrane signals vary with the particle moving along membrane nanotube (n = 14). The color bar indicates an intensity bar from 0 to 255. The white rectangular areas indicate that the max intensity of the DiO signals varies over time. The time format is minutes:seconds. (f−i) Time-lapse imaging illustrates QDs-WGAs (the arrows) can merge together (blue arrow) to move toward the target cell (h) (n = 23) and then merge and spilt at random near the target cell (g) (n = 7). The time format is minutes:seconds. The similar merging and splitting process also occurred in the white circle region in panel f (see Supporting Information Movie S4). (h) The y position of the particles (the arrows in panel f) *vs* time plots indicates that the particles merge together on the membrane nanotube. (i) The y position of the particles (the arrows in panel g) *vs* time plots show the merging and splitting process. The scale bars represent 2 μm in panels b, e, f, and g.

internalized into cancer cells.[26,27] Additionally, the merge image of QDs and DiO signals (Figure 2d) showed that QDs-WGA was in the nanotubes between A549 cells (n > 100). In a reconstruction of the fluorescence images of A549 cells in three dimensions, the profile image (Figure 2e) and the orthogonal slice view (Figure 2f) of the nanotubes further elaborated that the nanotube was just like a "flyover" on the substratum and the QDs-WGA was in the connecting membrane nanotubes between A549 cells (see Supporting Information, Movie S1).

Motion Behaviors of QDs-WGA in Membrane Nanotubes. To investigate whether membrane nanotube could be utilized for the cell-to-cell transportation, real-time monitoring of the transport behaviors of nanotubes between A549 cells was performed for long-term (n > 100). By two-color single-particle tracking, we found that QDs-WGA could be transported along the nanotubes between two cells. The snapshots and the whole trajectory of a particle (Figure 2g, h and see Supporting Information, Movie S2) showed that the particle was leaving one cell body, moving ahead along the nanotube, and then reaching the other cell for about 6 min. This proved that the membrane nanotubes could facilitate intercellular transfer. The velocity and distance to origin *vs* time plots indicated that the transport of QDs-WGA is slow and unidirectional in a membrane nanotube (Figure 2i). This is inconsistent with the movements of vesicles and QDs, which were considered as a microtubule-based traffic in a stepwise, bidirectional manner.[5,24] Furthermore, we analyzed the movements of QDs-WGA in the nanotube, according to the relationship between mean square displacement ($\langle\Delta r^2\rangle$) and time (Δt) (Figure 2j). The apparent upward curve suggested that the movements could be characterized as directed motion along cytoskeletons.[25,28] The diffusion coefficient and fitting velocity were 0.001 $\mu m^2/s$ and 0.033 μm/s, consistent with the values of actin-based movements.[29] It was speculated that QDs-WGA may be propelled by actin filaments. The particular motion behaviors implied that the transport of nanoparticles in nanotubes was diverse from cell types.

Subsequently, concerns had been raised about how multiple particles moved in the nanotube. By time-lapse imaging, we observed that multiple particles could be transported in the same nanotube in special ways. A systematic analysis of QDs-WGA particles in nanotubes showed two different types of moving behaviors: (i) moving in concert; and (ii) moving into conflict.

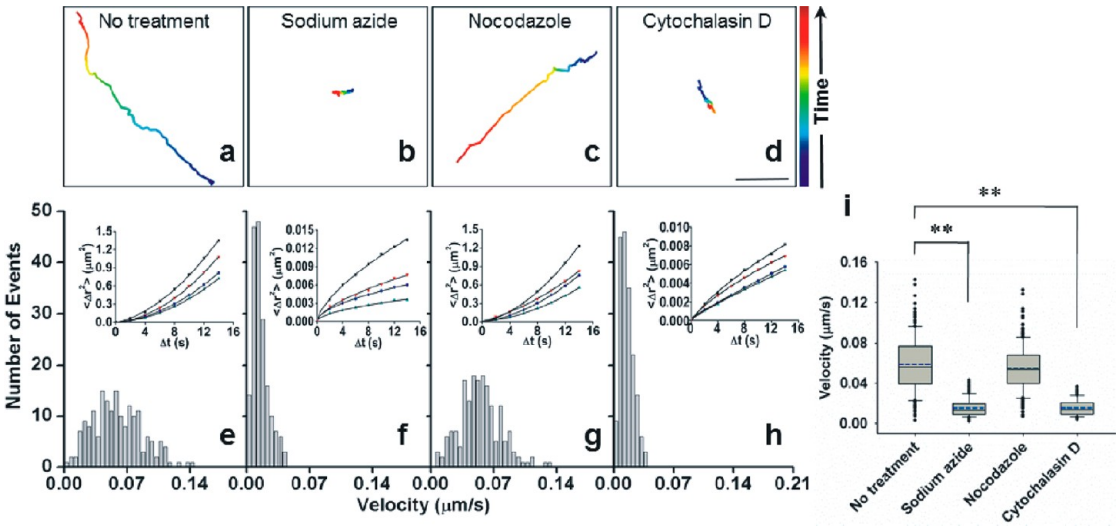

Figure 4. Transport of QDs-WGA in membrane nanotubes is an active and actin-dependent process. (a−d) Shown are typical trajectories of the 240 s of QDs-WGA moving along nanotubes in untreated, sodium azide-treated (see Supporting Information Movie S5), nocodazole-treated (see Supporting Information Movie S6), and cytochalasin D-treated cells (see Supporting Information Movie S7), respectively. The color bar indicates a time axis from 0 (blue) to 240 s (red). (e−h) Histograms depict the distributions of the instantaneous velocities of QDs-WGA moving along nanotubes in untreated (mean ± s.d., 0.059 ± 0.028 μm/s), sodium azide-treated (0.015 ± 0.009 μm/s), nocodazole-treated (0.055 ± 0.023 μm/s), and cytochalasin D-treated cells (0.015 ± 0.008 μm/s) (n = 180 per group). The insets illustrate $\langle \Delta r^2 \rangle$ *vs* Δt plots (color symbols) of the QDs-WGA moving along nanotube under the different conditions. The lines of the insets (e and g) are the fits to $\langle \Delta r^2 \rangle = 4D\Delta t + (V\Delta t)^2 +$ constant. The lines of the insets (f and h) are the fits to $\langle \Delta r^2 \rangle = 4D\Delta t^{\alpha} +$ constant. (α is a coefficient, $\alpha < 1$, and the constant term is due to noise) (i) Box plots indicate the instantaneous velocity of QDs-WGA moving along membrane nanotubes under the different conditions (n = 180 per group). Double asterisks, $P < 0.01$. The scale bar represents 2 μm in panels a−d.

As shown in Figure 3a,b, the snapshot and kymograph image of three particles in a nanotube demonstrated that two particles were moving in the same direction, but another one was moving in the opposite direction (see Supporting Information, Movie S3) (n = 15). The distance to origin *versus* time plots indicated that the transport of particles were all unidirectional, but in different directions (Figure 3c). By statistical analysis (P = 0.76, one-way ANOVA), the box plots of the velocities showed that there was no significant difference between the velocities of the three particles (Figure 3d), suggesting that the transport behaviors in the nanotubes were independent of the diversity of particles. Besides, we observed an interesting phenomenon, when a traffic collision occurred between particles in the nanotubes. The particles in a nanotube were moving in different directions, and merging together, followed by a coherent motion toward the cell body (Figure 3f,g and Supporting Information, Movie S4) (n = 23). This implied that the parallel motions of particles may not occur in the nanotubes. Interestingly, when a more detailed observation was performed on the merged particle near the target cell body, we found that the splitting and merging process occurred at random (Figure 3g). The y position of the particles *versus* time plots further illustrated the dynamic unstable state of the particle, indicating that the merging behaviors in the nanotube will be a special way for facilitating particles transport, based on the particular topology of the nanotube (Figure 3h,i). Additionally, it was notable that the plasma membrane in some nanotubes was flowing with the moving of particles and the thick nanotube became a thin one (n = 14) (Figure 3e). This phenomenon showed striking similarities to the disassembly of the nanotube in human macrophages,[5] suggesting that the apparent retraction of the nanotube may be a way of rupture of the nanotubes accompanied with intercellular transport (Supporting Information, Figure S4).

Transportation of QDs-WGA Driven by Myosin Molecular Motors. To get more in-depth exploration of the transport mechanism of QDs-WGA in membrane nanotubes, we monitored the movements of QDs-WGA in cells treated with sodium azide (an ATP-depletion drug), nocodazole (a microtubule-disrupting drug), and cytochalasin D (an actin-depolymerizing drug,) respectively. In the same time period, the trajectory in nocodazole-treated cell (Figure 4c, see Supporting Information, Movie S6) was very similar to that in an untreated cell (Figure 4a). In striking contrast, the movements in sodium azide or cytochalasin D-treated cells were markedly limited (Figure 4b,d, see Supporting Information, Movie S5 and Movie S7).The distribution of the instantaneous velocities showed that the movements in untreated (mean ± s.d., 0.059 ± 0.028 μm/s, Figure 4e) or nocodazole-treated cells (0.055 ± 0.023 μm/s, Figure 4g) were much faster than that in sodium azide (0.015 ± 0.009 μm/s, Figure 4f) or cytochalasin D-treated cells (0.015 ± 0.008 μm/s, Figure 4h) (n = 180 per group), demonstrating that the movements were strongly inhibited due to ATP depletion or actin depolymerizing. Meanwhile, the $\langle \Delta r^2 \rangle$ *vs* Δt plots of four

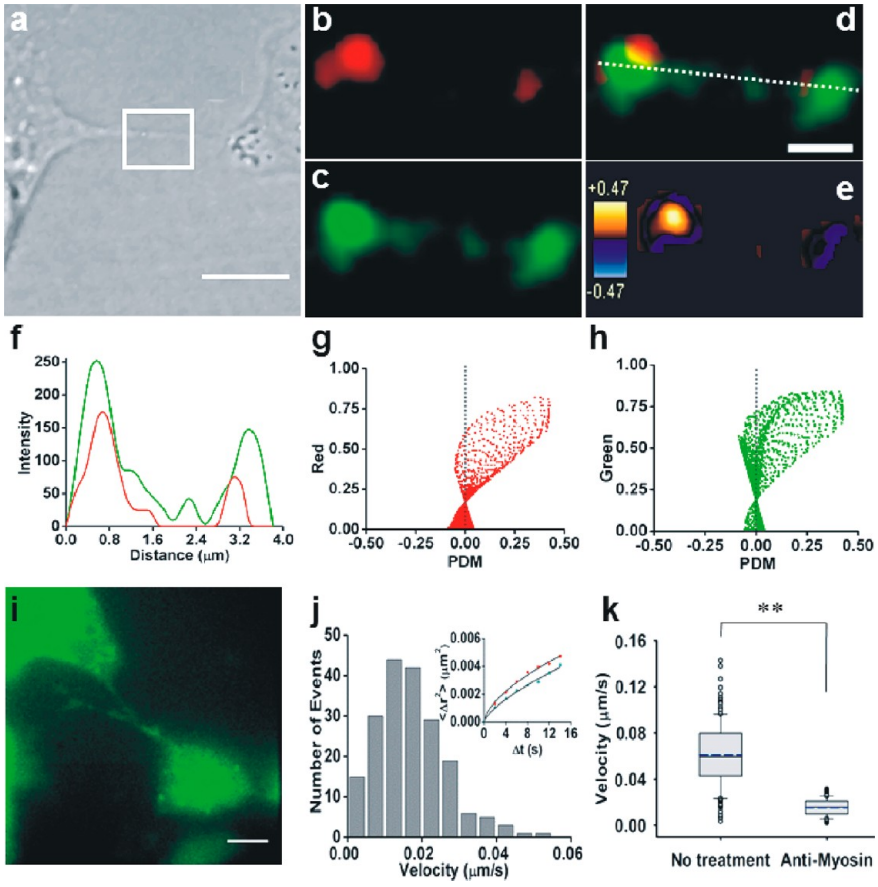

Figure 5. Myosin motors drive QDs-WGA transport in nanotube. (a−h) Immunofluorescence assay and intensity correction analysis reveal that QDs-WGA colocalized with myosin partially. (a) Shown is bright-field image of nanotube between A549 cells. The cells preincubated with QDs-WGA were immunolabeled with the antibody against myosin. For the boxed region, fluorescence images of QDs-WGA (b), myosin motors, (c) and the merge (d) are magnified to better visualize the nanotube. By intensity correlation analysis, the product of the differences from the mean (PDM) image (e) and intensity correlation plots of QDs-WGA (g, red) and myosin (h, greed) are obtained for analyzing the colocalization extent (intensity correction quotient, 0.34). (f) The cross-line scan of the fluorescence intensities of the merge image (the white line shown in panel d) exhibits the distribution of myosin motors (green) and WGA (red) signals. (i−k) Microinjection method further confirms that QDs-WGA transport is driven by myosin motor (see Supporting Information Movie S8). (i) Myosin antibody (green) was microinjected into the cells which connected by nanotubes. (j) The histogram depicts the distribution of instantaneous velocities of QDs-WGA moving on nanotubes between the microinjected cells (mean ± s.d., 0.015 ± 0.007 μm/s) (n = 180). The inset shows $\langle \Delta r^2 \rangle$ *vs* Δt plots (color symbols) of the QDs-WGA moving along the nanotube between the microinjected cells. The black lines are the fits to $\langle \Delta r^2 \rangle = 4D\Delta t^{\alpha} +$ constant. (k) Box plots indicate the instantaneous velocity of QDs-WGA moving along the membrane nanotubes between the normal cells and microinjected cells, respectively (n = 180 per group). Double asterisks, $P < 0.01$. The scale bars represent 10 μm in panels a and i and 1 μm in panels b−e.

typical trajectories in each group (inset in Figure 4e−h) suggested that the movements in nocodazole-treated cells were directed and indistinguishable from the untreated cell. The $\langle \Delta r^2 \rangle$ *vs* Δt downward plots showed that the movements were confined in the nanotubes after ATP depletion or actin depolymerizing. By statistical analysis (Two-Sample *t*-Test, Figure 4i), box plots of velocities of particles under the different conditions showed that the movements were significantly inhibited in sodium azide ($P < 0.01$) and cytochalasin D-treated cells ($P < 0.01$). The above results indicated that the transfer of QDs-WGA in membrane nanotubes was a unidirectional and actin-driven active movement.

Contrary to the bidirectional transport model propelled by kinesin and/or dynein motors,[30] the movement of QDs-WGA may be identical with an actomyosin-dependent transport system, such as in TNT-like bridges.[3,31] To determine whether QDs-WGA movements in membrane nanotubes were associated with myosin motors, we immunostained myosin motors with antimyosin antibody in A549 cells preincubated with QDs-WGA. It was evident that myosin motors and QDs-WGA were present in the membrane nanotubes (Figure 5a−d). Utilizing intensity correlation analysis (ICA), the product of the differences from the mean (PDM) image (Figure 5e) and intensity correlation plots (Figure 5g,h) showed that the QD signals were colocalized with myosin signals. By quantitative analysis, the Mander's coefficient (tMR and tMG, colocalization coefficients for red and green signals in thresholded images, respectively) and the intensity correlation quotient (ICQ) values were 0.97, 0.62, and 0.34 respectively,

further demonstrating that most QDs were indeed colocalized with myosin motors. The line profile of the cell showed that the QD signals were always accompanied by the myosin signals, confirming that WGA movements were bound up with myosin motors (Figure 5f). To better elucidate the relationship between QDs-WGA movements and myosin motors, we microinjected antimyosin antibody into the adjacent cells which were connected by a membrane nanotube (Figure 5i). Videomicroscopic analysis showed that the movement of QDs-WGA was strongly inhibited and the velocity sharply decreased to 0.015 ± 0.007 μm/s (n = 180) (Figure 5j and see Supporting Information, Movie S8). From statistical analysis (Two-Sample t-Test), the motion behaviors of QDs-WGA in the nanotubes exhibited significant difference ($P < 0.01$) compared with that in untreated cells (Figure 5k). The $\langle \Delta r^2 \rangle$ *vs* Δt plots displayed the apparent downward curvature, suggesting QDs-WGA was moving confinedly in nanotube after microinjection. These results confirmed that QDs-WGA was propelled by myosin motors in membrane nanotubes. Comparison of the velocities in the unidirectional way with those in the bidirectional model[24] showed that the significant difference of movements was closely related to molecular motors associated with transportation in nanotubes, rather than the heterogeneity in nanotube structures.

CONCLUSION

Despite extensive efforts in investigating the membrane nanotube-mediated intercellular transportation,[20,21] many questions about the transport mechanism of membrane nanotubes between cancer cells are still poorly understood. Also largely unknown is whether the nanotubes could be used as the drug delivery channel for cancer therapy. In this study, we realized the real-time tracking of QDs-WGA in nanotubes over long-term, which allowed us to determine the transport mechanism of nanotubes and to explain directly how QDs-WGA moves in the nanotube for intercellular transportation.

Using single-particle tracking, we first visualized the entire transfer process of QDs-WGA in nanotubes between cancer cells. Our data demonstrated that the nanotubes allowed unidirectional transfer of QDs-WGA. By analyzing the motion behaviors of QDs-WGA, we proposed that the transport of QDs-WGA *via* membrane nanotubes is driven by myosin motors, inconsistent with the bidirectional transport model propelled by kinesin and/or dynein motors. The results showed that the significant difference of movements was closely related to molecular motors associated with transportation in nanotubes, rather than the heterogeneity in nanotube structures.

According to previous reports, membrane nanotubes could facilitate direct intercellular communication between cancer cells and provide a unique channel for intercellular transfer of cellular contents.[12,13] This indicated that nanotubes may also play an important role in carcinogensis and raised the question of whether it is possible to utilize membrane nanotubes for cancer therapy. Our results presented here proved that the exogenous drug carrier was effectively transported in membrane nanotubes between cancer cells. Hence, membrane nanotubes may open a new avenue for studying the intercellular communication between cancer cells and potential applications in cancer therapy. As a young research field, the further study on the formation, structure, function, and transport mechanism of membrane nanotubes is sorely needed for cancer research. In summary, we revealed the transport mechanism of membrane nanotubes between cancer cells. Our research on membrane nanotubes could provide a better understanding of cell-to-cell communication for cancer research and may lead to new insights into cancer metastasis

MATERIALS AND METHODS

Cell Culture and QDs Labeling. Human lung carcinoma (A549) cells were plated on a 35 mm glass-bottom Petri dish (NEST Corp) and grown in culture medium (DMEM, containing 10% fetal bovine serum, (Gibco), 100 units/mL penicillin G sodium and 100 μg/mL streptomycin sulfate) at 37 °C in a 5% CO_2 atmosphere for 24−48 h before the experiments. WGA was labeled with QDs by a two-step method reported previously.[25,32,33] Briefly, the cells were incubated with 2 nM biotinylated WGA (Vector Laboratories) in Tyrode's plus buffer, and then maintained with 2 nM SA-QDs (Wuhan Jiayuan Quantum Dots Co. LTD), followed by fluorescence imaging. Control experiments were carried out at the same conditions without biotinylated WGA in Tyrode's plus buffer.

Dye Staining and Immunofluorescence Labeling. To stain the cytomembrane of live A549 cells, 5 μg/mL 3,3′-dioctadecyloxacarbocyanine perchlorate (DiO) (Beyotime Institute of Biotechnology, Invitrogen) was added directly to the culture medium for 20 min at 37 °C. For labeling actin filaments and microtubules, immunofluorescence experiments were performed as follows. First, the cells were washed with phosphate-buffered saline (PBS) and fixed with 4% (w/v) paraformaldehyde for 20 min at room temperature. Subsequently, the cells were exposed in PBS containing 5% (w/v) BSA and 0.1% (w/v) Triton X-100 for 30 min. Then, phalloidin-FITC (Beyotime Institute of Biotechnology) was added to label F-actin. Tubulin-alpha monoclonal antibody (Abnova) and Dylight 649-conjugated goat antimouse IgG (Thermo) were used to stain microtubules. Myosin was labeled with mouse monoclonal to myosin (Abcom) and Dylight 488-conjugated goat antimouse IgG (Thermo) using the method mentioned above.

Drug Inhibition. All drug inhibition experiments were performed after incubating the cells with QDs-WGA. For the ATP-depletion experiments, the cells were exposed in Tyrode's plus buffer with 50 mM 2-deoxy-D-glucose (sigma) and 10 mM sodium azide (sigma) for 30 min at 37 °C.[34] To disrupt actin filaments and microtubules, the cells were incubated with 20 μM cytochalasin D and 60 μM nocodazole (Sigma) for 30 min at 37 °C, respectively.[29] During the experiments, the cells were always immersed in the Tyrode's plus buffer with drugs.

Microinjection. An Eppendorf TransferMan NK2 micromanipulator and an Eppendorf FemtoJet injection system (Eppendorf AG, Germany) were utilized for microinjection. Capillaries were prepared with a model P-2000 capillary puller (Sutter Instruments Co., USA). The cells preincubated with QDs-WGA were monitored using a fluorescence microscope (Axiovert 200M, Carl Zeiss) and microinjected with ~20 fl mouse monoclonal to myosin (0.1 mg/mL) based on standard procedures. FITC was used to denote the microinjected cells. Next, the cells were cultured for 30 min at 37 °C and then imaged by confocal microscopy.

Fluorescence Imaging. Fluorescence images were acquired using a spinning-disk confocal microscope (Andor Revolution XD) with an Olympus IX 81 microscope, a Nipkow disk-type confocal unit (CSU 22, Yokogawa), a cell culture system (INUBG2-PI), and an EMCCD (Andor iXon DV885K). DiO/Dylight 488, QDs and Dylight 649 were excited at 488 nm, 561 and 640 nm by DPSS lasers, respectively. Using 525/50 nm, 617/73 nm, and 685/40 nm bandpass emission filters, the emission was split into different channels. For simultaneous multiple-color imaging, the fluorescence was detected separately with the EMCCD by appropriate channels.

Imaging Analysis. Each frame of the movies was denoised by using a Gauss filter, and the orthogonal slice view was obtained by Andor IQ software (Andor Technology). All images were restored with the deconvolution algorithm. The tracking of QDs-WGA was performed with Imaging-Pro-Plus software (Media Cybernetics Inc. USA). Mean squared displacement was calculated for each time interval over a trajectory with the user-written program.[28] ICA was performed with a plug-in for Image J.[35] An intensity correlation quotient (ICQ) and Mander's coefficient (tMR and tMG, above threshold) were quantitatively calculated to examine the extent of colocalization of QDs with myosin motors in membrane nanotubes.[36] The tMR value denoted the overlap percentage of red on green, and the tMG value indicated the overlap percentage of green on red. The PDM image and intensity correlation plots were obtained for visualizing the colocalization level by ICA. Line profile of the signals in the membrane nanotubes was exhibited by using Image Pro Plus software.

Statistical Analysis. AVNON or Two-Sample *t*-Test was utilized for statistical tests.

Conflict of Interest: The authors declare no competing financial interest.

Acknowledgment. This work was supported by the National Basic Research Program of China (973 Program, No. 2011CB9-33600), the Science Fund for Creative Research Groups of NSFC (No. 20921062), the National Natural Science Foundation of China (20833006, 21005056), and the "3551 Talent Program" of the Administrative Committee of East Lake Hi-Tech Development Zone ([2011]137).

Supporting Information Available: Figures S1−S4 and Movies S1−S8 as described in the text. This material is available free of charge *via* the Internet at http://pubs.acs.org.

REFERENCES AND NOTES

1. Holder, J. W.; Elmore, E.; Barrett, J. C. Gap Junction Function and Cancer. *Cancer Res.* **1993**, *53*, 3475–3485.
2. Naus, C. C.; Laird, D. W. Implications and Challenges of Connexin Connections to Cancer. *Nat. Rev. Cancer* **2010**, *10*, 435–441.
3. Rustom, A.; Saffrich, R.; Markovic, I.; Walther, P.; Gerdes, H. H. Nanotubular Highways for Intercellular Organelle Transport. *Science* **2004**, *303*, 1007–1010.
4. Smith, I. F.; Shuai, J.; Parker, I. Active Generation and Propagation of Ca^{2+} Signals within Tunneling Membrane Nanotubes. *Biophys. J.* **2011**, *100*, L37–L39.
5. Onfelt, B.; Nedvetzki, S.; Benninger, R. K.; Purbhoo, M. A.; Sowinski, S.; Hume, A. N.; Seabra, M. C.; Neil, M. A.; French, P. M.; Davis, D. M. Structurally Distinct Membrane Nanotubes between Human Macrophages Support Long-Distance Vesicular Traffic or Surfing of Bacteria. *J. Immunol.* **2006**, *177*, 8476–8483.
6. Sowinski, S.; Jolly, C.; Berninghausen, O.; Purbhoo, M. A.; Chauveau, A.; Köhler, K.; Oddos, S.; Eissmann, P.; Brodsky, F. M.; Hopkins, C.; *et al.* Membrane Nanotubes Physically Connect T Cells Over Long Distances Presenting a Novel Route for HIV-1 Transmission. *Nat. Cell Biol.* **2008**, *10*, 211–219.
7. Gousset, K.; Schiff, E.; Langevin, C.; Marijanovic, Z.; Caputo, A.; Browman, D. T.; Chenouard, N.; de Chaumont, F.; Martino, A.; Enninga, J.; *et al.* Prions Hijack Tunnelling Nanotubes for Intercellular Spread. *Nat. Cell Biol.* **2009**, *11*, 328–336.
8. Sherer, N. M.; Lehmann, M. J.; Jimenez-Soto, L. F.; Horensavitz, C.; Pypaert, M.; Mothes, W. Retroviruses Can Establish Filopodial Bridges for Efficient Cell-to-Cell Transmission. *Nat. Cell Biol.* **2007**, *9*, 310–315.
9. Watkins, S. C.; Salter, R. D. Functional Connectivity between Immune Cells Mediated by Tunneling Nanotubules. *Immunity* **2005**, *23*, 309–318.
10. Chauveau, A.; Aucher, A.; Eissmann, P.; Vivier, E.; Davis, D. M. Membrane Nanotubes Facilitate Long-Distance Interactions between Natural Killer Cells and Target Cells. *Proc. Natl Acad. Sci. U.S.A.* **2010**, *107*, 5545–5550.
11. Chinnery, H. R.; Pearlman, E.; McMenamin, P. G. Cutting Edge: Membrane Nanotubes *in Vivo*: A Feature of MHC Class II^+ Cells in the Mouse Corneal. *J. Immunol.* **2008**, *180*, 5779–5783.
12. Vidulescu, C.; Clejan, S.; O'Connor, K. C. Vesicle Traffic through Intercellular Bridges in DU 145 Human Prostate Cancer Cells. *J. Cell. Mol. Med.* **2004**, *8*, 388–396.
13. Lou, E.; Fujisawa, S.; Morozov, A.; Barlas, A.; Romin, Y.; Dogan, Y.; Gholami, S.; Moreira, A. L. Tunneling Nanotubes Provide a Unique Conduit for Intercellular Transfer of Cellular Contents in Human Malignant Pleural Mesothelioma. *PLoS ONE* **2012**, 7.
14. Lochner, N.; Pittner, F.; Wirth, M.; Gabor, F. Wheat Germ Agglutinin Binds to the Epidermal Growth Factor Receptor of Artificial Caco-2 Membranes as Detected by Silver Nanoparticle Enhanced Fluorescence. *Pharm. Res.* **2003**, *20*, 833–839.
15. Gabor, F.; Bogner, E.; Weissenboeck, A.; Wirth, M. The Lectin-Cell Interaction and Its Implications to Intestinal Lectin-Mediated Drug Delivery. *Adv. Drug Delivery Rev.* **2004**, *56*, 459–480.
16. Liu, B.; Bian, H. j.; Bao, J. k. Plant Lectins: Potential Antineoplastic Drugs from Bench to Clinic. *Cancer Lett.* **2010**, *287*, 1–12.
17. Niemeyer, C. M. Nanoparticles, Proteins, and Nucleic Acids: Biotechnology Meets Materials Science. *Angew. Chem. Int. Ed.* **2001**, *40*, 4128–4158.
18. Chan, W. C. W.; Maxwell, D. J.; Gao, X. H.; Bailey, R. E.; Han, M. Y.; Nie, S. M. Luminescent Quantum Dots for Multiplexed Biological Detection and Imaging. *Curr. Opin. Cell Biol.* **2002**, *13*, 40–46.
19. Medintz, I. L.; Uyeda, H. T.; Goldman, E. R.; Mattoussi, H. Quantum Dot Bioconjugates for Imaging, Labelling and Sensing. *Nat. Mater.* **2005**, *4*, 435–446.
20. Davis, D. M.; Sowinski, S. Membrane Nanotubes: Dynamic Long-Distance Connections between Animal Cells. *Nat. Rev. Mol. Cell Biol.* **2008**, *9*, 431–436.
21. Gerdes, H. H.; Carvalho, R. N. Intercellular Transfer Mediated by Tunneling Nanotubes. *Curr. Opin. Cell Biol.* **2008**, *20*, 470–475.
22. Doherty, G. J.; McMahon, H. T. Mediation, Modulation, and Consequences of Membrane−Cytoskeleton Interactions. *Annu. Rev. Biophys* **2008**, *37*, 65–95.
23. Pontes, B.; Viana, N. B.; Campanati, L.; Farina, M.; Neto, V. M.; Nussenzveig, H. M. Structure and Elastic Properties of Tunneling Nanotubes. *Eur. Biophys. J.* **2008**, *37*, 121–129.
24. He, K.; Luo, W.; Zhang, Y.; Liu, F.; Liu, D.; Xu, L.; Qin, L.; Xiong, C.; Lu, Z.; Fang, X.; *et al.* Intercellular Transportation of Quantum Dots Mediated by Membrane Nanotubes. *ACS Nano* **2010**, *4*, 3015–3022.
25. Liu, S. L.; Zhang, Z. L.; Sun, E. Z.; Peng, J.; Xie, M.; Tian, Z. Q.; Lin, Y.; Pang, D. W. Visualizing the Endocytic and Exocytic Processes of Wheat Germ Agglutinin by Quantum Dot-Based Single-Particle Tracking. *Biomaterials* **2011**, *32*, 7616–7624.
26. Wu, X. Y.; Liu, H. J.; Liu, J. Q.; Haley, K. N.; Treadway, J. A.; Larson, J. P.; Ge, N. F.; Peale, F.; Bruchez, M. P.

Immunofluorescent Labeling of Cancer Marker Her2 and Other Cellular Targets with Semiconductor Quantum Dots. *Nat. Biotechnol.* **2003**, *21*, 41–46.
27. Howarth, M.; Takao, K.; Hayashi, Y.; Ting, A. Y. Targeting Quantum Dots to Surface Proteins in Living Cells with Biotin Ligase. *Proc. Natl. Acad. Sci. U.S.A.* **2005**, *102*, 7583–7588.
28. Saxton, M. J.; Jacobson, K. Single-Particle Tracking: Applications to Membrane Dynamics. *Annu. Rev. Biophys. Biomol. Struct.* **1997**, *26*, 373–399.
29. Lakadamyali, M.; Rust, M. J.; Babcock, H. P.; Zhuang, X. W. Visualizing Infection of Individual Influenza Viruses. *Proc. Natl Acad. Sci. U.S.A.* **2003**, *100*, 9280–9285.
30. Kuznetsov, A. V. Modeling Bidirectional Transport of Quantum Dot Nanoparticles in Membrane Nanotubes. *Math. Biosci.* **2011**, *232*, 101–109.
31. Zhu, D. H.; Tan, K. S.; Zhang, X. L.; Sun, A. Y.; Sun, G. Y.; Lee, J. C. M. Hydrogen Peroxide Alters Membrane and Cytoskeleton Properties and Increases Intercellular Connections in Astrocytes. *J. Cell Sci.* **2005**, *118*, 3695–3703.
32. Lidke, D. S.; Nagy, P.; Heintzmann, R.; Arndt-Jovin, D. J.; Post, J. N.; Grecco, H. E.; Jares-Erijman, E. A.; Jovin, T. M. Quantum Dot Ligands Provide New Insights into ErbB/HER Receptor-Mediated Signal Transduction. *Nat. Biotechnol.* **2004**, *22*, 198–203.
33. Liu, S. L.; Zhang, Z. L.; Tian, Z. Q.; Zhao, H. S.; Liu, H.; Sun, E. Z.; Xiao, G. F.; Zhang, W.; Wang, H. Z.; Pang, D. W. Effectively and Efficiently Dissecting the Infection of Influenza Virus by Quantum-Dot-Based Single-Particle Tracking. *ACS Nano* **2012**, *6*, 141–150.
34. Kam, N. W. S.; Liu, Z. A.; Dai, H. J. Carbon Nanotubes as Intracellular Transporters for Proteins and DNA: An Investigation of the Uptake Mechanism and Pathway. *Angew. Chem. Int. Ed.* **2006**, *45*, 577–581.
35. Li, Q.; Lau, A.; Morris, T. J.; Guo, L.; Fordyce, C. B.; Stanley, E. F. A Syntaxin 1, G alpha(o), and N-Type Calcium Channel Complex at a Presynaptic Nerve Terminal: Analysis by Quantitative Immunocolocalization. *J. Neurosci.* **2004**, *24*, 4070–4081.
36. Melemedjian, O. K.; Asiedu, M. N.; Tillu, D. V.; Peebles, K. A.; Yan, J.; Ertz, N.; Dussor, G. O.; Price, T. J. IL-6-and NGF-Induced Rapid Control of Protein Synthesis and Nociceptive Plasticity *via* Convergent Signaling to the EIF4F Complex. *J. Neurosci.* **2010**, *30*, 15113–15123.